CETRA2024 15-17 May 2024, Cavtat, Croatia
8th International Conferenceon Road and Rail Infrastructure

DEVELOPMENT OF CONTACT STRESSES ON RAILS AND THE NEED FOR SPECIALLY GRADED STEEL FOR RAILWAYS

Niyazi Özgür Bezgin
Istanbul University – Cerrahpaşa, Turkey

Abstract

Between the wheels of the train and the rails, there exist variable and triaxial stresses that include the vertical stresses, longitudinal stresses, and lateral stresses generated by the vertical, longitudinal, and lateral forces exerted by the train wheels on the rails. In addition to these stresses, there are residual in-plane and longitudinal stresses within the rails generated during their production and longitudinal stresses generated by ambient temperatures on continuously welded rails. The simultaneous presence of many types of stresses on rails with varying magnitudes that can be quite high generates unusual mechanical demands from the rails as opposed to other types of structural elements of civil engineering, which require special cross-sectional designs and metallurgical constituency. The type and magnitude of stresses along a railway route vary with the locations along the route with higher stresses along the acceleration and deceleration zones within and near the stations, horizontal curves, slopes, stiffness transition zones and turnouts. This study provides analytical insight into the magnitudes of vertical, longitudinal, and lateral forces that can occur at the wheel and rail interface and the analytical means to estimate these forces. The study later elaborates on the stresses that these forces can generate on the railhead and highlights the need for high-strength rail steel along railway routes and special rail profiles along curves.

Keywords: railhead, contact stresses, Nadal's equation, conicity, tribology

1 Introduction

Mechanics of railway track superstructures is an elaborate field of structural engineering research that involves a wide spectrum of research areas that include but are not limited to tribology, contact mechanics, metallurgy, soil and structure interaction, and structural dynamics [1]. Rail steels have higher strength, hardness, and corrosion resistance requirements compared to ordinary steel structures encountered in civil engineering. The rails are exposed to triaxial stresses together with abrasion and fatigue in addition to locked-in stresses during their production [2]. With that comes a variety of peculiar strength, ductility, and hardness requirements that the rails must meet. This paper partly addresses these requirements through an analytical assessment of the vertical forces, lateral forces, and longitudinal forces that act at the rail and wheel interface. The first part of this study includes an analytical assessment of the varying vertical forces on the rails along a track curve, followed by an assessment of the lateral force limits on a train along a curve by revisiting the Nadal criteria for train derailment [3, 4]. The final section involves an analytical assessment of the wheel and rail contact stresses through the Hertz Theorem to comment on the magnitude of the stresses that arise at the wheel and rail interface that implicates the need for high strength and specially alloyed steel for rails.

DOI: https://doi.org/10.5592/CO/CETRA.2024.1519

2 Development of rail reactions to a train negotiating a curve

Figure 1 presents the lateral and vertical forces within the cross-section of the train perpendicular to its longitudinal axis.

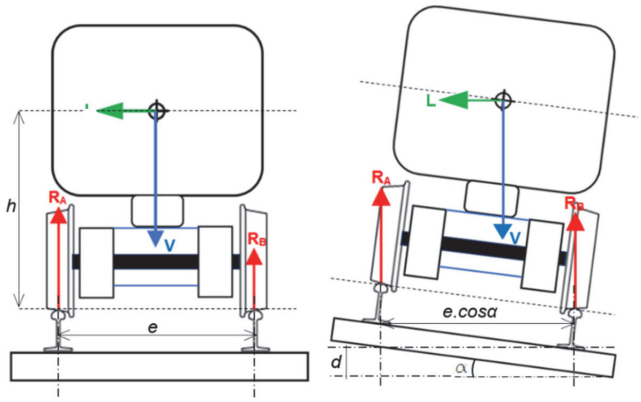

Figure 1 Vertical and horizontal forces and rail reactions on a train body

As a train negotiates a track curve, a centripetal force acts towards the center of the curve to keep the train along the curve. This force is provided by the friction and bearing forces at the wheel and rail interface provided by the embedment bearing and friction forces of the railway track frame with its supporting structure. The inertia to this force, called the centrifugal force (L), equal in value opposes the direction of the centripetal force as long as the centripetal force lasts and directly relates to the square of the train speed (v) and inversely relates to the curve radius (r). A set of two axle-mounted train wheels is a common unit for investigating the forces transferred by the train to the track. The heaviest axle of the train set, likely to provide traction in addition to transferring the forces generated by its supported tributary mass, is the representative of the train in terms of its mechanical interaction with the track. The tributary weight of the train (V) representing the vertical force on a representative axle act at the center of gravity (CG) of the representative tributary train mass supported by that axle. The width of the track is 'e' and the height of the CG to the top of the track (TOR) is 'h'. Tributary train mass is composed of the train body, the bogie (truck), and the axle-wheel configuration. Figure 1 does not show the centripetal force, lateral reactions, and longitudinal traction forces at the TOR.

Equations 1 to 4 show the vertical reaction forces, R_A and R_B, as represented in Figure 1. Equations (3) and (4) reduce to $R_A = R_B = V/2$ for a straight track (r = infinite), without any cant (d = 0).

$$R_A + R_B = V \tag{1}$$

$$R_A \cdot \cos\alpha \cdot e = V \cdot \cos\alpha \cdot \frac{e}{2} - V \cdot \sin\alpha \cdot h + L \cdot \cos\alpha \cdot h + L \cdot \sin\alpha \cdot \frac{e}{2} \tag{2}$$

$$R_A = V\left(\frac{1}{2} - \tan\alpha \cdot \frac{h}{e}\right) + L\left(\frac{h}{e} + \frac{\tan\alpha}{2}\right) \tag{3}$$

$$R_B = V\left(\frac{1}{2} + \tan\alpha . \frac{h}{e}\right) - L\left(\frac{h}{e} - \frac{\tan\alpha}{2}\right) \tag{4}$$

To limit the net centrifugal acceleration experienced by the passengers within the train body or the goods within the body of a freight train, the track is tilted toward the center of the curve center. The track along the curve is given a "cant" (d) to the outer rail above the horizontal axis, providing a "cant angle" (α) with the lateral TOR axis of the track. The so-called "theoretical cant angle", $a_{teo,}$ and "theoretical cant", d_{teo} is the cant value that induces a zero net lateral acceleration on the train mass and is given by the analytical developments introduced through Equations (5) to (8).

$$V \cdot \sin\alpha_{teo} = L \cdot \cos\alpha_{teo} \tag{5}$$

$$m \cdot g \cdot \sin\alpha_{teo} = m \cdot \frac{v^2}{r} \cdot \cos\alpha_{teo} \tag{6}$$

$$\tan\alpha_{teo} = \frac{v^2}{r \cdot g} \rightarrow \alpha_{teo} = \operatorname{atan}\left(\frac{v^2}{r \cdot g}\right) \tag{7}$$

$$d_{teo} = e \cdot \sin\alpha_{teo} = e \cdot \sin\left[\operatorname{atan}\left(\frac{v^2}{r \cdot g}\right)\right] \tag{8}$$

For small angles up to and equal to a = 7°, sina~tana~a; which is valid for up to a thousandth, Equation (8) can be approximated with Equation (9). However, for larger angles, which is typically the case for the theoretical cant, Equation 8 gives results with higher precision.

$$d_{teo} \sim \frac{v^2 \cdot e}{r \cdot g} \tag{9}$$

Although the net lateral acceleration is zero at the theoretical cant, the cant value where $R_A = R_B = V/2$ along a curve is slightly higher than the theoretical cant. If one considers Equations 3 and 4, this equality occurs when the condition shown in Equation (10) is met.

$$V \cdot \tan\alpha \cdot \frac{h}{e} = L\left(\frac{h}{e} + \frac{\tan\alpha}{2}\right) \rightarrow m \cdot g \cdot \tan\alpha \cdot \frac{h}{e} = \frac{m \cdot v^2}{r}\left(\frac{h}{e} + \frac{\tan\alpha}{2}\right) \tag{10}$$

The cant angle α and d, where $R_A = R_B = V/2$ is given in Equations (11) and (12). Compared to Equation (8), Equation (12) gives a somewhat different result, which also depends on "h".

$$\alpha = \operatorname{atan}\left(\frac{\frac{v^2}{r} \cdot \frac{h}{e}}{\frac{g \cdot h}{e} - \frac{v^2}{2r}}\right) \tag{11}$$

$$d = e \cdot \sin\left[\operatorname{atan}\left(\frac{\frac{v^2}{r} \cdot \frac{h}{e}}{\frac{g \cdot h}{e} - \frac{v^2}{2r}}\right)\right] \tag{12}$$

Theoretical cant is typically a high value and cannot be used in practice. The cant used in design (d_{des}) is lower than d_{teo}. Therefore, a certain amount of cant reduction is included in the design that results in a 'cant deficiency', which leads to an acceptable or tolerable amount of net lateral acceleration in the mass of the train and passengers [5]. Equation (10) shows the relation between the cant values.

$$d_{def} = d_{teo} - d_{des} \tag{10}$$

Figure 2a presents the variation of R_A and R_B and Figure 2b presents the variation of net lateral acceleration with variable cant values for a static axle force value of F_s = 180 kN, for a static tributary mass of m = 18,349 kg, train speed v = 250 km/h, width of a normal gauge track e = 1500 mm, for cant values of d = 0, 50,100,150, 200, 250, 289, 320 mm. Curve radius is r = 2500 m. The theoretical cant when the net lateral acceleration is zero is d_{teo} = 289 mm and the cant value when $R_A = R_B$ is d = 320 mm.

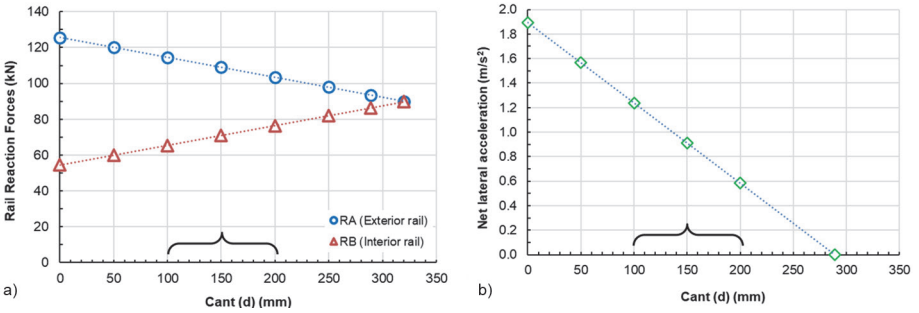

Figure 2 (a) Variation of the vertical reaction of the rails with cant, and (b) Variation of the net lateral acceleration with cant

Typical design cant values along railways typically vary between d_{des} = 100 mm – 200 mm. This indicates that there is always a higher vertical force along the outer rail along the track curves. The allowable values of net lateral acceleration typically vary between a_{net} = 0.65 – 1.0 m/s² [5]. The cant deficiency for a d_{des} = 150 mm is d_{def} = 139 mm, resulting in a net lateral acceleration of a_{net} = 0.9 m/s². This net acceleration results in a net lateral force of L = 16.7 kN. For the condition presented in Figure 2, a 150mm design cant results in R_A = 110 kN for the outer rail and R_B = 70 kN for the inner rail. This difference is quite substantial and shows that the stress levels on the outer rails are higher than on the inner rails. A track curve with the design cant value will always have the outer rail stressed more heavily compared to the inner rail, due to the net lateral acceleration that develops due to cant deficiency and the design speeds unless the train stops at a curve (v = 0). Figure 3a shows that if the train stops at a curve (v = 0), the internal rail will be stressed more heavily. If the train travels at a speed lower than the design speed (v = 170 km / h), as shown in Figure 3b, the vertical forces on the rail heads can be equalized at d_{des} = 150 mm, but that would defeat the purpose of designing the curve for a train service at the dedicated service speed of v_{des} = 250 km/h.

The next section provides information on the Nadal Train Derailment Criteria that limits the lateral force (L) that the train can exert on the track to prevent derailment by causing the wheels to climb over the track with the traction of the flange to the railhead.

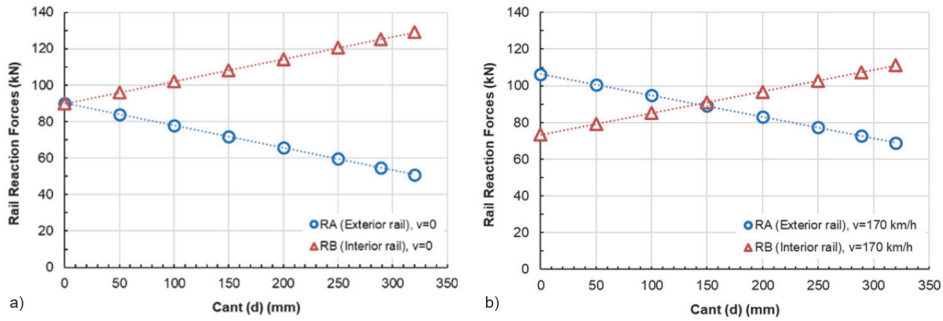

Figure 3 (a) Variation of the vertical reactions of the rails at v = 0 km/h, (b) Variation of the vertical reactions of the rails at v = 170 km/h

3 Nadal's derailment criteria and lateral force limit

Guidance of the trains along the railway is managed through the conicity of the train wheels; which will not be elaborated in this paper, and the wheel flanges. The interaction of the rolling surface of the wheels and the railhead is limited to a roughly 25 mm wide section on both surfaces. Design tolerances, deviations in track profile, and track and wheel roughness that can develop in time can disrupt the desired interaction, and there can be many accounts of wheel slippage and flange abrasion to the head. The lateral forces generated at the wheel and rail interface can cause the flanges to bear onto the railhead thus generating frictional forces that can cause the wheel to climb over the rail.

Both the railhead and the wheel thread have intricate design dimensions (x). These dimensions have evolved over time through extensive analytical and observational research concerning the interaction of the wheel with the railhead along track tangents and track curvatures. Details of these geometric details are beyond the scope of this paper and are the subject of a dedicated book on the matter. However, Figures 4a and 4b highlight a fundamental value for the wheel flange known as the 'flange angle'. The flange angle is measured roughly 10 mm below the tip of the flange that is approximately 25 mm deep. The minimum recommended angle of the flange is 72° [7]. Together with the dynamic friction coefficient "f" of the steel wheel and steel rail interface, the flange angle is important parameter in the determination of the lateral force limit that can cause a derailment. Figure 4c shows the forces that form a closed polygon at the wheel-and-rail contact interface.

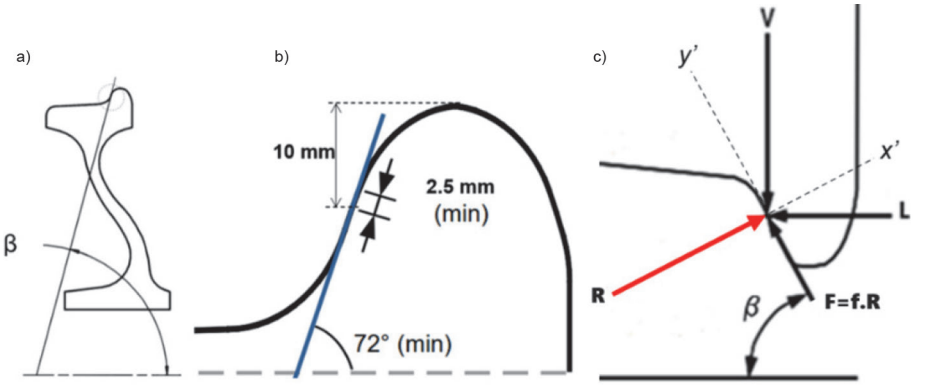

Figure 4 (a) Flange angle of a train wheel, (b) Measurement of the flange angle, (c) Lateral, vertical, frictional and resultant normal force at the flange-rail contact [6]

Figure 4c shows the force equilibrium at the wheel and rail contact point. The normal force N is the vectoral sum of L, V, and F. Wheel climbing occurs when the forces directed towards the *+y'* direction becomes greater than the forces directed towards the *-y'* direction. Therefore, the balance of forces along the y' direction must satisfy the equality presented in Equation (11).

$$f \cdot \sum F_{x'} = F < \sum F_{y} \tag{11}$$

Equations (11) and (12) present the sum of the forces along the respective axis.

$$\sum F_{x'} = V \cdot \cos\beta + L \cdot \sin\beta \tag{12}$$

$$\sum F_{y'} = V \cdot \sin\beta - L \cdot \cos\beta \tag{13}$$

Since the Nadal Criteria for Derailment interests itself with the ratio of the lateral force to the vertical force at the wheel and rail contact point, together with the L/V parameter, Equation 14 relates the friction coefficient f to the summation of the forces presented as L/V along the respective axis and the flange angle.

$$f < \frac{\sum F_{y'}}{\sum F_{x'}} = \frac{V \cdot \sin\beta - L \cdot \cos\beta}{V \cdot \cos\beta + L \cdot \sin\beta} = \frac{\sin\beta - \left(\frac{L}{V}\right) \cdot \cos\beta}{\cos\beta + \left(\frac{L}{V}\right) \sin\beta} \tag{14}$$

Resolution of Equation (14) to yield an L/V term results in Equation (15), which is Nadal's criterion for derailment [3].

$$\frac{L}{V} < \frac{\sin\beta - f \cdot \cos\beta}{f \cdot \sin\beta + \cos\beta} \tag{15}$$

Figure 5 presents a vector depiction of the forces at the wheel and rail contact point at the flange. The right-hand figure shows the force polygon showing the resultant force N and N' exerted onto the rail by the flange. The combined vectors L and V begin to generate a compressive force at the contact point that initiates a friction force that develops into its final value F. The final compressive force pressing onto the railhead is N. Since as the wheel rolls around its normal rolling contact area, denoted by the regional area R, the sideways wheel motion may occasionally force the wheel to contact the flange. Because the wheel cannot roll around both contact points simultaneously, friction occurs at the contact point with the flange. As the lateral force on the railhead increases, so does the resulting friction F and the N vector increases in magnitude and rotates clockwise around the contact point. Finally, there comes a point when the N' vector passes over the horizontal axis along which the L' vector is positioned, generating an upward pull on the wheel that the rail can no longer resists. In other words, the upward forces along the y' axis overcome the downward forces along the y'axis, and the wheel flange climbs over the rail. With increasing L and F, there comes a point when N is no longer downward but upwards; a direction that is not stable. This is the point of derailment.

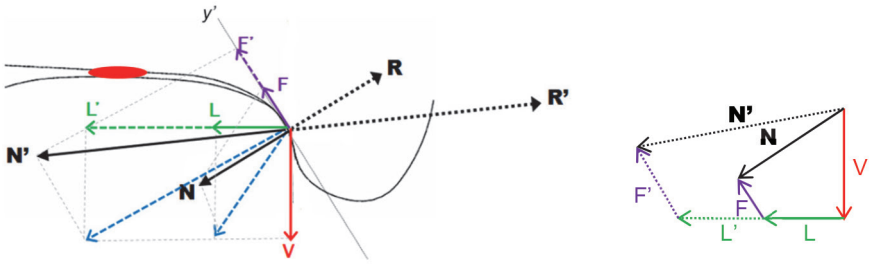

Figure 5 Vectoral presentation of forces at wheel and rail contact point and the force polygon

Figure 5 provides a simplified presentation of the wheel flange and rail contact. The actual conditions are far more complicated with the angle of attack of the wheel to the rail, the degrading flange angle in time and the primary stiffness of the bogie (truck) which are not considered in this study. However, the figure is instructive in terms of the forces in the plane that contribute to the conditions for derailing. The friction force (F) along the plane of the flange angle, which may change in time, relates to the component of the resultant force (V+L+F) that is perpendicular to the flange angle and the coefficient of dynamic friction constant between the flange and the wheel. The wear of the wheel flange frequently results in a reduction in the angle of the flange. Therefore, railway service providers include this fact in their considerations for limiting the lateral force limit that can be imposed on the railway track. To this end, UIC leaflet 518 specifies a limit of 0.8 in the L/V ratio that takes into account adverse friction conditions at the wheel-rail interface and the deteriorated angle of the wheel flange [7]. Figure 6 shows the variation of L/V with flange angle and the dynamic coefficient of friction between the rail and wheel flange interface. Increasing friction at the wheel flange and rail interface and reduced flange angles are detrimental to the allowable lateral force limit on the track. Dynamic friction coefficients represent a spectrum ranging from wet rail-to-wheel flange interaction to dry and corroded wheel-to-flange interaction. For the hypothetical case study presented in this study, the outer wheel force of R_A = 110 kN would require L = 0.8 x 110 kN = 88 kN to initiate the derailment according to the UIC limit.

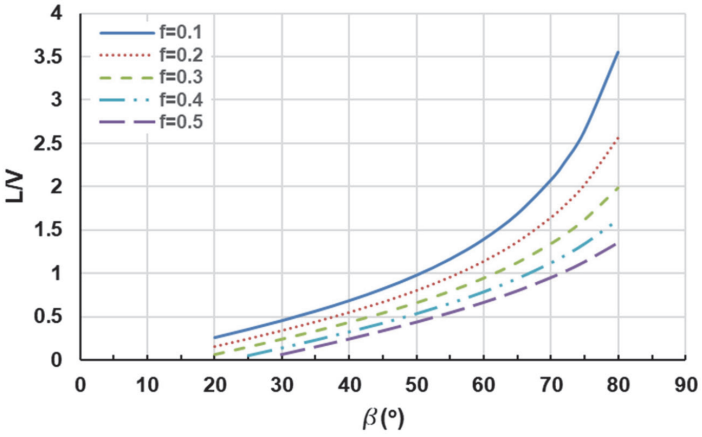

Figure 6 Variation of L/V with b and f

4 Contact stresses at the wheel and rail interface

Together with the vertical force of the wheel on the rail, the lateral and longitudinal stresses exerted on the rail generate a triaxial state of stresses at the wheel and rail contact point. Train wheels and track wheels are composed of specially alloyed high-strength steel with hardened contact interfaces. Together with the curved contact surfaces, their mutually bearing areas are extremely limited in size to 1-2 cm^2. Hertzian theory is developed to investigate the stresses in such bearing conditions due to normal loading [8]. The approximated elliptical contact patch between the bearing surfaces leads to an array of equations that describe the contact pressures for the varying curvatures of the bearing elements. Kalker's theory, includes the tangential loadings that occur at the contact points in addition to the normal loads [9]. The breadth and depth of studies concerning the contact mechanics of high-rigidity curved surfaces is extensive and can be traced back to studies that began as early as the 1880s. This section will portray the state of triaxial forces on the wheel and rail contact point and elaborate on the type and magnitude of stresses that can develop at the wheel and rail contact interface.

Traction along the rail is dependent on the static friction available at the wheel-rail contact interface. For a dry rail to dry wheel contact, a static friction constant of $f_s = 0.25$ [9]. Slippage of the wheel over the rail reduces the effect friction at the interface to its dynamic value, which can be $f_d = 0.2$. For the 180 kN static axle force introduced in the first section, the static vertical wheel force on a rail along a tangent is V = 90 kN. Due to the small cant angle, the cosine of which is very close to 1, the exact vertical force component on the railhead is taken equivalent to V. The traction force that this wheel can extract from its contact with the rail is $T = V \times f_s = 90$ kN x 0.25 = 22.5 kN. However, along a curve with $d_{des} = 150$ mm, the outer rail received a higher vertical wheel load of V = 110 kN, as shown in Figure 3a. Therefore, the outer rail of a curve will be stressed to a higher level than the rail along the tangent. The traction force on the outer rail of a curve can be as high as T = V x fs = 110 kN x 0.25 = 27.5 kN. In addition to this traction force, the net lateral acceleration, $a_{net} = 0.912$ m/s^2 generated a centrifugal force $2L = m \times a_{net} = 18{,}349$ kg x 0.912 m/s^2 = 16.8 kN on the train body, which also increased the force on the outer rail. This force is transferred to the rails, which resist laterally by the interface friction. Unless the wheels slide laterally and engage the outer wheel flange with the head of the rail, for all practical purposes, it can be assumed that this force is evenly distributed between the two rails L = 8.4 kN. Since L is lower than the traction force T, the flanges for this particular case will not engage with the rail head.

One addition to the discussion above would be the dynamic impact force (DIF). The static values of the vertical forces above typically increase with a dynamic impact factor. Railway agencies try to limit this increase in service conditions to a certain level such as DIF = 1.2. If this factor increases beyond the allowable range, track and rolling stock maintenance protocols begin to remedy the cause that generates high dynamic impact forces. Therefore, based on the values of the case study presented in this article, the state of the vertical forces on a rail varies from a minimum of V = 90 kN for a train at standstill on a tangent, to a dynamic vertical force of V = 1.2 x 90 kN = 108 kN along a tangent, to V = 1.2 x 110 kN = 132 kN along a curve. In addition to these vertical forces, there are traction forces and lateral forces. As the train accelerates along a tangent, such as departure from a station or decelerates along a tangent, such as an approach to a station, the biaxial state of the forces, including the vertical dynamic impact forces, would be V = 108 kN and T = 22.5 kN. Since dynamic impact forces are temporary, the static value of vertical wheel force is included to estimate the traction force. If the train accelerates along a curve, the triaxial state of the forces on the railhead is V = 132 kN, T = 27.5 kN and L = 8.4 kN. At an additional extreme, such that the lateral force exerted on the track is the limit lateral force described by the Nadal Criteria, L = 0.8 x V = 0.8 x 110 kN = 88 kN, which is a tremendous increase from the lateral force value during ordinary service.

Figure 8a shows a typical 60E1 type rail cross section [10]. The figure 7 shows that the railhead profile varies from a radius of 300 mm along the rolling band of the railhead to 80 mm and then to 13 mm at the railhead corners. Figure 7 (right) shows the strength grades of a particular type of rails [10].
Normal contact stresses between the curved surface of the steel rail and the curved surface of the steel wheel, which has a diameter of 920 mm for this study, can be studied with the Hertzian contact theorem. Under the conditions of elastic behavior and frictionless contact, semi-infinite spaces, large contact radii compared to contact area dimensions and constant curvature, Hertz demonstrates that the contact area of the two rigid surfaces is an ellipse with a semiellipsoid pressure distribution. Equation (18) shows the Hertzian contact stresses at the contact point of two rigid curved bodies [8].

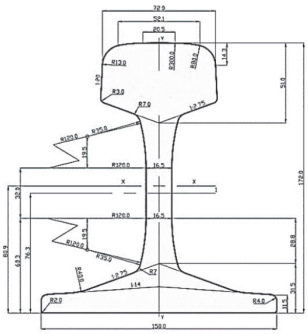

STANDARD	STEEL GRADE	MECHANICAL PROPERTIES		
		RM M PA	MIN A5%	HB
UIC 860-R	700	680 830	14	-
	900A	880 1030	10	-
	900B	880 1030	10	-
EN 13674-1	R200	MIN 680	14	200-240
	R260	MIN 880	10	260-300
	R260 MN	MIN 880	10	260-300
	R350 HT	MIN 1175	9	350-390
	R350 LHT	MIN 1175	9	350-390
EN 13674-2	R260	MIN 880	10	260-300
	R350 HT	MIN 1175	9	350-390
	R350 LHT	MIN 1175	9	350-390
BS 11 1965	A	MIN 880	8	-
	B	MIN 880	8	-
AREMA	CARBON STANDARD CARBON HIGH STRENGTH	MIN 983 MIN 1179	10 10	MIN 310 STANDARD S. RAIL MIN 370 HIGH S. RAIL
	LOW ALLOY INT. STRENGTH LOW ALLOY HIGH STRENGTH	MIN 1014 MIN 1179	8 10	MIN 325 INTERMEDIATE S. RAIL MIN 370 HIGH S. RAIL
AS 1085.1	ALL RAIL	MIN 880	8	MIN 260
	MICROALLOYED	780 1130	9	MIN 340
AM	900ACRV	MIN 1040	9	320-360
	B1000	MIN 966	9	MIN 315
	900ACRV	MIN 1080	9	320-360

Figure 7 60E1 rail profile and particular rail strength grades [10]

$$p(x,y) = \frac{3f_n}{2\pi ab}\sqrt{1-\frac{x^2}{a^2}-\frac{y^2}{b^2}} \tag{18}$$

$$a = m\sqrt[3]{\frac{3(1-\kappa^2)f_n}{E(A+B)}},\ b = n\sqrt[3]{\frac{3(1-\kappa^2)f_n}{E(A+B)}}$$

The propriety software HertzWin 3.1.1 performs Hertzian stress analyses for rigid body contact that include normal forces and traction [11]. The particular application of the generalized equation given in Equation (18) to rails and train wheels yields Equation (19) where b is half the width of the elliptical contact patch and r is the radius of the wheel [12].

$$p_{max} = \frac{3}{2}\sqrt{\frac{\pi \cdot E}{64\left(1-\vartheta^2\right)}\cdot\frac{V}{r.b}} \tag{19}$$

Under the ordinary and desired contact of the wheel with a radius of 460 mm with the rail at the head of the rail with a contact radius of 300 mm, the estimated normal Hertzian compressive stresses and the shear stresses that arise under varying vertical forces are depicted in Figure 3a based on the results extracted from the software. The Hertzian contact stress results given by the program are approximately 22% higher than the results obtained by Equation (19) which only considers the radius of the wheel but not the contact radius of the railhead. Figure 8b shows the variation of Hertzian and shear stresses with depth below the wheen and rail contact.

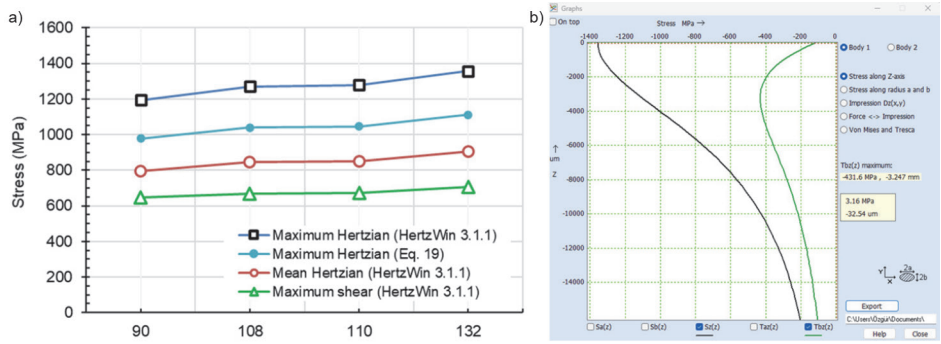

Figure 8 (a) Hertzian contact stresses and related shear stresses and (b) their variation with depth

Figure 9 shows the stress analyzes performed on the contact surfaces, depicting the simultaneous application of the Hertzian contact stresses and the imposed traction and lateral stresses.

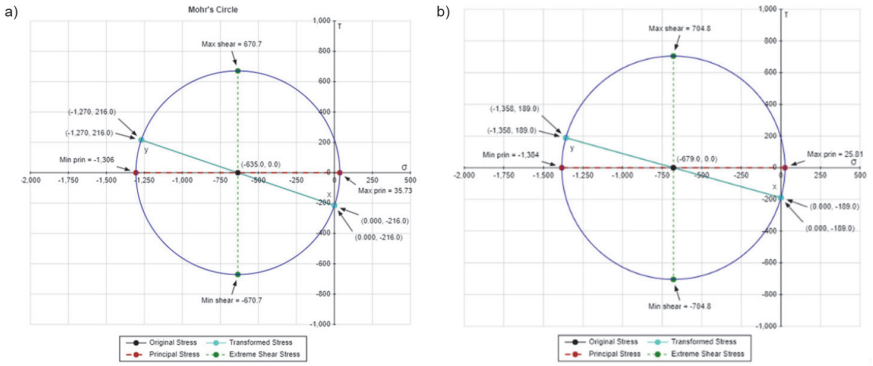

Figure 9 Variation of stresses due to the triaxial state of the imposed stresses

Figure 10 presents a representation of the stresses that would occur if the elements in contact remained in their elastic stress regions. The interaction of the wheel flange with the railhead edge with 13 mm diameter generates very high stresses that plastifies and eventually depletes the strength of the steel surrounding the contact area. With repeated contact, the damage to the contacting steel elements progresses. The Hertzian approach, which assumes that the material behavior is elastic, estimates very high stresses that could not occur, since they greatly exceed the tensile strength of the wheel and rail steels. However, these high values are indicative of the fact that extensive abrasion and material losses will occur at the flange and rail interface. Layers of material from both the rail and the wheel are shed as the contacting materials work harden and then fracture microscopically with each passage of the train wheels.

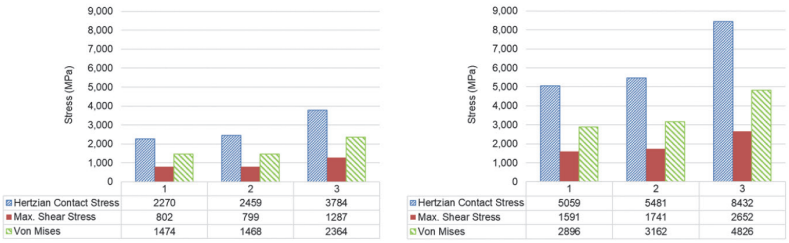

Figure 10 Extreme magnitude of estimated stresses based on elastic contact assumption that cannot be upheld, thus indicating plastification and material loss

At this extreme, where the wheel flange is in contact with the railhead corner, under extreme circumstances, damage on both the track and the rail is definite, the development rate of which depends mainly on the tonnage on the track and the track maintenance conditions. Figure 11 present sketches of worn rail and wheel profiles along track curves under extreme contact stress conditions [13].

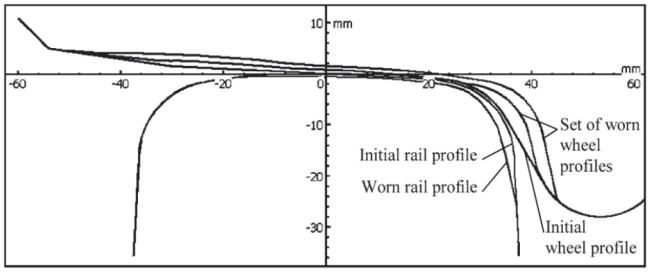

Figure 11 The worn wheel profile and the worn rail profile depiction [13]

Table 1 provides a summary of the investigated track conditions and the results stresses. The double-underlined values indicate extremely high stresses based on elastic analyses that cannot be reached. Therefore, these values indicate material plastification and hence failure. High compressive Hertzian contact stresses can be tolerated to a certain level because the stress deformation characteristics of steel under tension and compression are different. However, the repetitive shear stresses that arise internally due to compressive stresses deplete the elastic response of the material, forcing it into the plastic domain and eventually causing internal fractures in addition to the high abrasive stresses that occur along the contact interface.

Table 1 List of wheel and rail contact conditions considered and stress assessments

Track zone and motion type		Rail contact radius (mm)	Forces (kN)			Stresses (MPa)		
			Vertical	Lateral	Traction	Hertz	Max. Shear	Von Mises
I	Acceleration and deceleration along a tangent with vertical dynamic impact	300	108	None	22.5	**1,376**	**437**	**851**
II	Acceleration and deceleration along a curve with vertical dynamic impact	300	132	8.4	22.5	**1,434**	**458**	**891**
		80	132	8.4	22.5	***2,399***	***782***	***1,439***
III	Nadal's lateral force limit along a curve with constant speed and vertical dynamic impact	13	132	88	None	***8,432***	***2,652***	***4,826***

5 Discussion and conclusions

Numerical analyses of the stresses within and below the contact patch exposed to a triaxial state of stress are complex, requiring iterative numerical solutions that take into account the varying profiles of both the wheels and rails that are stressed beyond their elastic limits. This study presented a simplified approach to assessing the stresses that can occur at the wheel and rail interface. The study first introduced the variation in vertical wheel forces along the curves of the railway track, highlighting the variation of vertical wheel forces on the railhead as they are exposed to lateral forces limited by the allowable net lateral accelerations. The study then revisited the Nadal Derailment Criteria and analytically redeveloped the equation to depict the limit of the lateral force on the railway tracks. Together with the longitudinal forces required for traction to accelerate and decelerate the trains, the study provided analytical insight into the triaxial state of forces on the railhead and the resulting stresses. Through a hypothetical case study that involved the 250 km/h service speed of a train with a representative 180 kN static axle force, with a design cant of 150 mm along a 2500 m radius curve and design DIF = 1.2, the study considered the developing forces on the track with variable flange angles and dynamic coefficients of interface friction. Through an elastic stress analysis through the Hertz Theorem and Mohr stress analyses, the study reached normal contact, shear stress, and Von Mises stress values, with varying magnitudes for different operational conditions along the track. These conditions included the static placement of the train on a track, accelerating train along a tangent track with dynamic impact forces, accelerating train along curve with dynamic impact forces and finally a train along a curve that has reached the lateral force limit described by Nadal.

The deceleration and acceleration zones that approach and recede a station are exposed to traction forces in addition to vertical wheel forces. The outer rails along the track curves are exposed to higher vertical forces due to net lateral acceleration and exposed lateral forces. Traction along curves induces a longitudinal force in addition to vertical and lateral forces, thus increasing the combined shear stress levels within the rails. The study of rigid body contact conditions of steel wheels and rails is a complex field of inquiry. The presented study aimed to provide a simplified insight into the magnitude of stresses that could occur under ordinary service conditions, highlighting the need for metallurgically advanced wheel and rail steels for the contact stresses that could occur.

References

[1] Iwnicki, S.: Handbook of Railway Dynamics, Taylor and Francis, 2006.

[2] Lichtberger, L.: Track Compendium. Eurail Press, 2011.

[3] Nadal, M.J.: Theorie de la Stabilite des locomotives, Part II: mouvement de lacet, Annales des Mines, 10 (1896), 232

[4] Popp, K., Schiehlen, W.: Ground Vehicle Dynamics, Springer, 2010.

[5] Deng, X., Shi, H., Guo, J., Zhu, H.: European high-speed bogie technology review, International Journal of Vehicle Design, *79* (2019) 1, pp. 43–62, DOI: 10.1504/IJVD.2019.10023091

[6] APTA PR-M-S-015-06, Rev. 1. Commuter, Intercity and High-Speed Rail Mechanical Working Group, Wheel Flange Angle for Passenger Equipment, 2022.

[7] UIC 518 (E) 4th Edition, September 2009.

[8] Heckmann, A., Keck, A., Kaiser, I., Kurzeck, B.: The Foundation of the DLR Railway Dynamics Library: The Wheel-Rail-Contact, German Aerospace Center (DLR), 10th Modelica Conference, Lund, Sweden, 10-12 March 2014.

[9] Iwnicki, J.E.: Vehicle Dynamics and the Wheel/Rail Interface, Rail Technology Unit, Manchester Metropolitan University, IMechE Seminar, London, April 2002.

[10] https://rails.arcelormittal.com/products/transport-rails

[11] https://vinksda.com/toolkit-release-notes-en/release-notes-of-hertzwin/

[12] Esveld, C.: Modern Railway Track, MRT-Productions, 2001.

[13] Kovalev, R. et. al.: Freight car models and their computer-aided dynamic analysis, Multibody Syst Dyn, 22 (2009), pp. 399-423, DOI: 10.1007/s11044-009-9170-6